Accurate Systematic Model-Parameter Extraction for On-Chip Spiral Inductors

Hao-Hui Chen, *Member, IEEE*, Huai-Wen Zhang, Shyh-Jong Chung, *Senior Member, IEEE*, Jen-Tsai Kuo, *Senior Member, IEEE*, and Tzung-Chi Wu

***Abstract*—A systematic model-parameter-extraction technique is presented for accurately modeling on-chip spiral inductors in radio frequency integrated circuits (RFICs). The model is a π-circuit with an additional parallel RC network connecting both vertical branches to account for substrate coupling. The extraction starts with extracting the series inductance and resistance at low frequencies. Then, the oxide capacitance is evaluated in an intermediate frequency range. Afterward, the substrate effects including the substrate resistance and capacitance, as well as coupling, are extracted at higher frequencies. All the lumped circuit element values are analytically determined by the network analysis from the measured network parameters (S- or Y-parameters). The proposed approach thus can provide better circuital interpretations of the inductor behaviors for facilitating the design of RFIC inductors. Square and circular CMOS spiral and octagonal BiCMOS7 spiral inductors are investigated to test this technique. Highly accurate frequency responses by the extracted parameters are obtained over a wide frequency band without any optimization. This reveals the validation and capability of the proposed parameter-extraction method.**

***Index Terms*—Inductor model, parameter extraction, spiral inductors.**

I. Introduction

With THE rapid growth of the demand for low-power, low-cost, and high-integration wireless communication systems, the development of on-chip passive devices for radio frequency integrated circuits (RFICs) has emerged as a critical issue recently. Among the passive circuit designs, on-chip spiral inductors are particularly important and widely used in RFICs such as mixers, low-noise amplifiers, and oscillators. To facilitate the circuit simulation and optimization of RFICs, various modern inductor models such as modified π-models [1]–[8], double-π models [9], [10], higher order intrinsic models [11], and T-models [12]–[14] have been developed to characterize RFIC inductors in a wide frequency band. As the circuit scheme of a comprehensive inductor model generally consists of several series and shunt branches, to accurately extract the circuit elements in such a complicated model is a challenging task. Physics-based formulation and quasi-static electromagnetic calculation have been proposed for evaluating the elements in the circuit model [2]–[4], [9]. However, the results predicted by these approaches are normally estimated solutions. A parameter-extraction technique based on measurement data is therefore indispensable for accurate extraction of the model parameters. Curve fitting approaches using various mathematical techniques such as genetic algorithm, particle swarm optimization, vector fitting procedure, and augmentation method have been applied to extract the model parameters from the measured data [8], [13]–[16]. In general, these mathematical treatments can greatly improve the model accuracy, but they often require considerable computing resources, as well as proper initial guesses to obtain accurately converged solutions. Moreover, it is difficult to acquire the related physical conceptions of the effects of model parameters on the inductor characteristics from these mathematics-based methodologies.

On the other hand, analytical extraction techniques based on the network analysis, such as those reported in [12]–[14] and [17]–[19], are much more efficient and capable of providing physical aspects of the inductor behaviors. In these analytical approaches, approximations that are valid at relatively low or high frequencies are usually utilized to decompose the complicated circuit model into several subcircuits. The elements are then extracted step by step from the simplified subcircuits. Although these network-based extraction techniques are effective and suitable for physical modeling, there are still challenges and need for further improvements. As mentioned earlier, the subcircuits treated in each extracting procedure are approximated results of the whole circuit model in certain frequency ranges. Determining the frequency bands applicable for the approximations would be an important concern to the accurate extraction of the element values. This critical issue, however, has not been given the attention it needs. Furthermore, even in the analysis of the simplified subcircuits, numerical manipulation and/or assumption, such as vector fitting [13], [14], iterative computation [18], power-series approximation [19], and symmetrical assumption [12], [18], [19], were often required to deal with the parameter extraction. Due to the errors stemmed from the approximations and numerical treatments applied in the extracting procedures, further optimization is generally required to improve the accuracy of the final results.

In this paper, an accurate systematic parameter-extraction technique for on-chip spiral inductors is presented. Fig. 1 shows the circuit model for inductors to be investigated. This model is

Manuscript received May 22, 2008; revised August 19, 2008. Current version published October 30, 2008. This work was supported in part by the MoE ATU program, Taiwan, and in part by the SRC program under Contract 2003-TJ-1090. The review of this paper was arranged by Editor V. R. Rao.

H.-H. Chen was with the Department of Electronic Engineering, Huafan University, Taipei 22301, Taiwan, R.O.C. He is now with the Department of Electronic Engineering, National Kaohsiung First University of Science and Technology, Kaohsiung 824, Taiwan, R.O.C. (e-mail: hhchen@huafan.hfu.edu.tw).

H.-W. Zhang is with the United Microelectronics Corporation, Hsinchu 300, Taiwan, R.O.C.

S.-J. Chung and J.-T. Kuo are with the Department of Communication Engineering, National Chiao Tung University, Hsinchu 300, Taiwan, R.O.C.

T.-C. Wu is with Inventec Corporation, Taoyuan 335, Taiwan, R.O.C.

Digital Object Identifier 10.1109/TED.2008.2005131

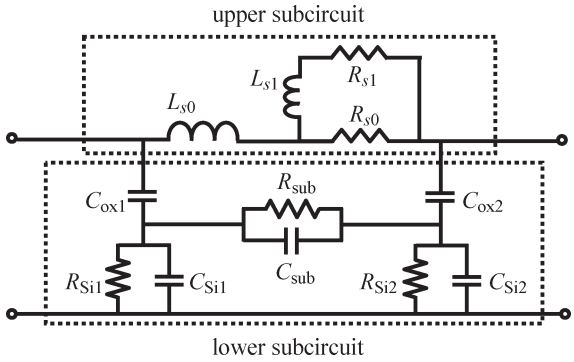

Fig. 1. Enhanced circuit model for on-chip spiral inductors.

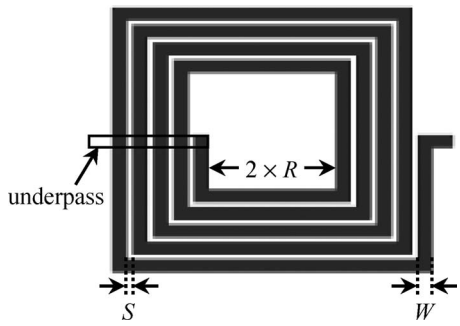

Fig. 2. Top view of the tested 4.5-turn square spiral inductor.

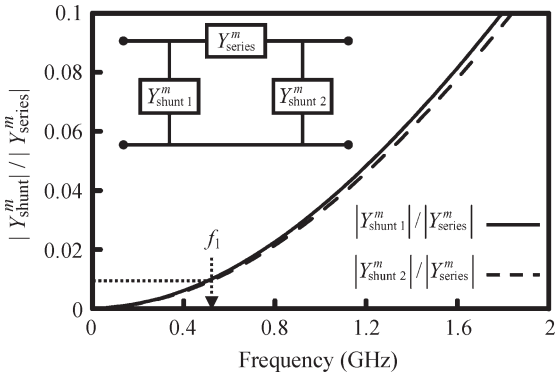

Fig. 3. Comparison of shunt and series admittances of the π-network for the inductor circuit.

first proposed in [1] and has been used in various RF circuit designs [20], [21]. It is named as the enhanced model herein. To extract the 12 elements in the model, the circuit is decomposed into several subcircuits based on suitable approximations in certain frequency ranges. By the network analysis of the simplified subcircuits, the series inductance and resistance of the spiral metal coil (L_{s0}, R_{s0}, L_{s1}, and R_{s1}) are first extracted from the measured Y-parameters at low frequencies. The oxide capacitance between the spiral and the silicon substrate ($C_{\rm ox1}$ and $C_{\rm ox2}$) is then evaluated in an intermediate frequency range. Afterward, the elements representing the substrate resistance ($R_{\rm Si1}$ and $R_{\rm Si2}$) and capacitance ($C_{\rm Si1}$ and $C_{\rm Si2}$), as well as the lateral coupling among the metal lines ($R_{\rm sub}$ and $C_{\rm sub}$) are extracted at higher frequencies. To mitigate the possible errors resulted from the approximations, the frequency bands suitable for the considered subcircuits are quantitatively determined by the Y-parameters. Such a procedure can also be utilized to assess the contributions of oxide and substrate parasitics at a specified operating frequency. It will be seen that the circuital equations for solving the model parameters derived in the proposed approach are very simple. No complex mathematical manipulation (such as vector fitting or iterative calculation) is required. The extraction is therefore very efficient and easy to be automatically implemented. Meanwhile, since the model parameters are analytically extracted by the network analysis, this technique can provide better circuital interpretations of the inductor behaviors for facilitating the RFIC inductor designs. Square and circular CMOS spiral and octagonal BiCMOS7 spiral inductors are used to test the presented technique. Highly accurate simulations by the extracted parameters are obtained over a wide frequency band without a need for further optimization, indicating the validation and capability of the proposed extraction method.

II. Parameter-Extraction Procedure

To illustrate the proposed parameter-extraction method, a 4.5-turn square spiral fabricated by the 0.18-μm 1P6M CMOS process with 2-μm top metal thickness is used as an example. Fig. 2 shows the top view of the inductor, where the linewidth (W), line spacing (S), and inner radius (R) are 14.5, 2, and 60 μm, respectively. The underpass is located on the metal-five layer. The substrate resistivity is approximately 10 $\Omega \cdot$ cm, and the thickness of the oxide dielectric is about 7.5 μm. It is noticed that this example has been investigated and characterized by the enhanced model in [1] and [19]. One can therefore objectively compare the results obtained by the proposed technique with the published data. Moreover, to obtain the measured network parameters (S- or Y-parameters) for performing the extraction, one notes that the enhanced model with the elements calculated by optimization can accurately simulate the measured S- and Y-parameters [1]. It would be reasonable to treat the results modeled by the optimized elements as the measured data. We thus utilize these pseudomeasurement results to extract the model parameters in the following.

A. Low-Frequency Approximation

As shown in Fig. 1, the enhanced model can be treated as a parallel combination of the upper and lower subcircuits. Due to the dc-blocking property of the oxide capacitances $C_{\rm ox1}$ and $C_{\rm ox2}$, one can remove the lower subcircuit and approximately characterize the inductor by the upper subcircuit at low frequencies. Such an approximation has been widely applied to find the series inductance and resistance in many literatures (e.g., [17]–[19]). To mitigate the errors resulted from the approximation, however, the upper frequency limit applicable to the approximation should be specified. For validation, a π-network shown in the inset of Fig. 3 is used to temporarily model the inductor. In the network, the series admittance $Y^m_{\rm series} = -Y^m_{12}$, and the two shunt ones $Y^m_{\rm shunt1} = Y^m_{11} + Y^m_{12}$ and $Y^m_{\rm shunt2} = Y^m_{22} + Y^m_{12}$, where Y^m_{11}, Y^m_{22}, and Y^m_{12} are the measured two-port Y-parameters of the entire inductor. Fig. 3 shows the

magnitudes of the shunt admittances normalized with respect to that of the series admittance. It can be observed that, the lower the frequency, the smaller are the normalized magnitudes and, thus, the better the shunt branches behave like an open path. The upper frequency limit f_1 can therefore be specified by sufficient small normalized magnitudes. Here, 1% is chosen as the upper bound of both magnitudes. For the particular example, $f_1 = 0.52$ GHz is obtained.

B. Extraction of L_{s0}, R_{s0}, L_{s1}, and R_{s1}

When $f \le f_1$, the upper subcircuit can approximately represent the entire inductor. The impedance Z_u of the series arm is then represented by the measured Y_{12}^m as $Z_u = R_u(\omega) + j\omega L_u(\omega) = \mathrm{Re}[-1/Y_{12}^m] + j\mathrm{Im}[-1/Y_{12}^m]$. Moreover, from simple network analysis, Z_u can be expressed in terms of the unknown elements L_{s0}, R_{s0}, L_{s1}, and R_{s1} as

$$R_u(\omega) = R_{s0}\frac{R_{s1}R_t + \omega^2 L_{s1}^2}{R_t^2 + \omega^2 L_{s1}^2}$$
$$L_u(\omega) = L_{s0} + \frac{R_{s0}^2 L_{s1}}{R_t^2 + \omega^2 L_{s1}^2} \tag{1}$$

where $R_t = R_{s0} + R_{s1}$. The dc resistance and inductance are then equal to (1) evaluated at $\omega = 0$

$$R_{\mathrm{dc}} = \frac{R_{s0}R_{s1}}{R_t} \qquad L_{\mathrm{dc}} = L_{s0} + \frac{R_{s0}^2 L_{s1}}{R_t^2}. \tag{2}$$

From (1) and (2), it can be readily verified that

$$R_u(\omega) - R_{\mathrm{dc}} = T\left(L_{\mathrm{dc}} - L_u(\omega)\right) \tag{3}$$
$$R_u(\omega) - R_{\mathrm{dc}} = M(1 + T^2/\omega^2)^{-1} \tag{4}$$

where

$$T = \frac{R_t}{L_{s1}} \qquad M = R_{s0} - R_{\mathrm{dc}}. \tag{5}$$

Note that $R_u(\omega)$ and $L_u(\omega)$ in (3) and (4) are obtained by the measured Y_{12}^m data, whereas R_{dc} and L_{dc} are determined by Y_{12}^m measured at the low frequency limit. Then, $R_u(\omega) - R_{\mathrm{dc}}$ as a function of $L_{\mathrm{dc}} - L_u(\omega)$ can be plotted as shown in Fig. 4(a). (The frequency is also labeled on the upper horizontal axis in Fig. 4 for reference). It can be observed that $R_u(\omega) - R_{\mathrm{dc}}$ is very close to a linear function of $L_{\mathrm{dc}} - L_u(\omega)$ for $f \le f_1$, and the coefficient T in (3) can then be computed from its slope. Moreover, it is worthy to note that, when frequency goes beyond about 0.75 GHz, where $|Y_{\mathrm{shunt1,2}}^m|/|Y_{\mathrm{series}}^m| \gtrsim 0.02$ (see Fig. 3), the variation of $R_u(\omega) - R_{dc}$ with regard to $L_{\mathrm{dc}} - L_u(\omega)$ gradually deviates from linear characteristics. Since the linear behavior exists only when the low-frequency approximation is effective, the value of $|Y_{\mathrm{shunt1,2}}^m|/|Y_{\mathrm{series}}^m|$ used to determine the upper frequency limit f_1 discussed in Section II-A should be limited to 0.02. This finding can serve as a guideline for the choice of the upper bound of $|Y_{\mathrm{shunt1,2}}^m|/|Y_{\mathrm{series}}^m|$ in determining the low-frequency band.

By the T value, $R_u(\omega) - R_{\mathrm{dc}}$ versus $(1 + T^2/\omega^2)^{-1}$ is shown in Fig. 4(b). A good linear dependence of $R_u(\omega) - R_{\mathrm{dc}}$ on $(1 + T^2/\omega^2)^{-1}$ is observed again for $f \le f_1$, and the coefficient M in (4) can then be evaluated by finding the slope. With the calculated coefficients T and M, and the measured R_{dc} and L_{dc}, the values of L_{s0}, R_{s0}, L_{s1}, and R_{s1} can then be calculated from (2) and (5) as

$$R_{s0} = M + R_{\mathrm{dc}} \tag{6a}$$
$$R_{s1} = \frac{R_{s0}R_{\mathrm{dc}}}{M} \tag{6b}$$
$$L_{s0} = L_{\mathrm{dc}} - \frac{M}{T} \tag{6c}$$
$$L_{s1} = \frac{R_{s0} + R_{s1}}{T}. \tag{6d}$$

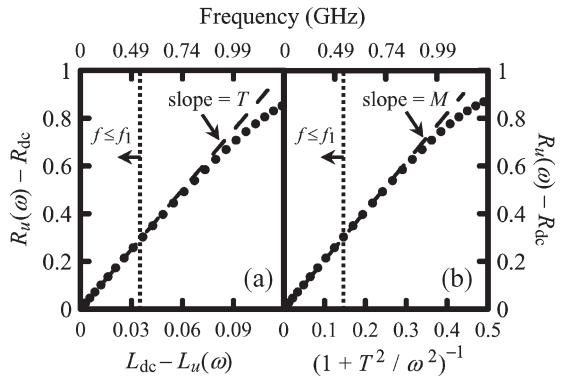

Fig. 4. $R_u(\omega) - R_{\mathrm{dc}}$ as functions of (a) $L_{\mathrm{dc}} - L_u(\omega)$ and (b) $(1 + T^2/\omega^2)^{-1}$. The slopes T and M are derived in the low frequency range $f \le f_1$.

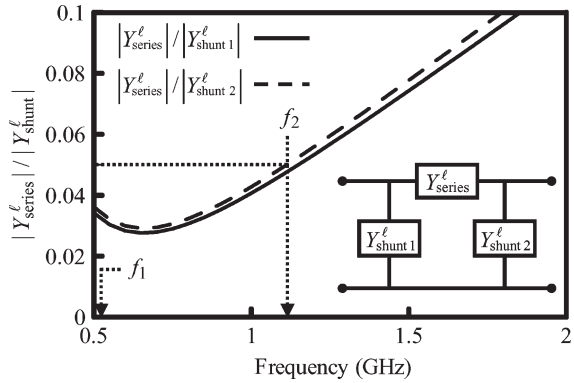

Fig. 5. Comparison of shunt and series admittances of the π-network for the lower subcircuit.

C. Extraction of C_{ox}

When $f > f_1$, the lower subcircuit has to be taken into account. Since the enhanced model is a parallel connection of the upper and lower subcircuits (see Fig. 1), the admittance Y-matrix of the lower subcircuit $[Y^{\ell}]$ can be then calculated as $[Y^{\ell}] = [Y^m] - [Y^u]$, where $[Y^m]$ is the measured Y-matrix of the entire inductor and $[Y^u]$ is that of the upper subcircuit which can be obtained once L_{s0}, R_{s0}, L_{s1}, and R_{s1} are known. By the matrix $[Y^{\ell}]$, an equivalent π-network with the series admittance $Y_{\mathrm{series}}^{\ell} = -Y_{12}^{\ell}$ and the shunt ones $Y_{\mathrm{shunt1}}^{\ell} = Y_{11}^{\ell} + Y_{12}^{\ell}$ and $Y_{\mathrm{shunt2}}^{\ell} = Y_{22}^{\ell} + Y_{12}^{\ell}$ is then constructed to characterize the lower subcircuit, where Y_{11}^{ℓ}, Y_{22}^{ℓ}, and Y_{12}^{ℓ} are the entries of $[Y^{\ell}]$. Fig. 5 shows the plot of the ratios $|Y_{\mathrm{series}}^{\ell}|/|Y_{\mathrm{shunt1,2}}^{\ell}|$

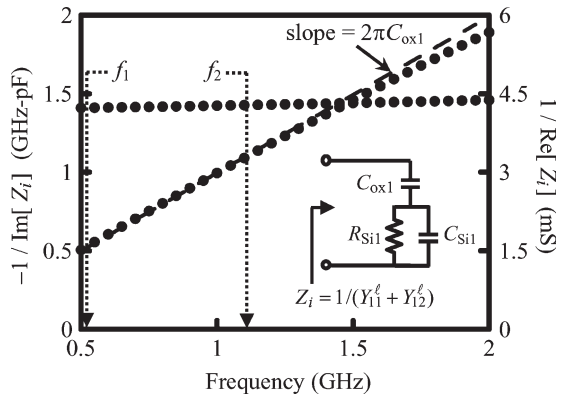

Fig. 6. $(-1/\mathrm{Im}[Z_i])$ and $(1/\mathrm{Re}[Z_i])$ as functions of frequency. The linear slope for $(-1/\mathrm{Im}[Z_i])$ is derived in the intermediate frequency range $f_1 \le f \le f_2$.

for 0.5 GHz $\le f \le$ 2 GHz. One can see that the ratios are much smaller than unity over the frequency band. A frequency f_2 below which $|Y^{\ell}_{\mathrm{series}}| \ll |Y^{\ell}_{\mathrm{shunt1}}|$ and $|Y^{\ell}_{\mathrm{shunt2}}|$ can be then defined to approximate the series branch as an open path. Here, 0.05 is adopted for the upper bound of the ratios to define f_2. Such a condition implies that the parallel network of R_{sub} and C_{sub} would behave like an open circuit in the intermediate frequency range $f_1 \le f \le f_2$, and the impedance of the left part of the lower subcircuit (see the inset of Fig. 6) can consequently be written as $Z_i = 1/(Y^{\ell}_{11} + Y^{\ell}_{12})$, which yields

$$\frac{1}{\mathrm{Re}\left[1/\left(Y^{\ell}_{11}+Y^{\ell}_{12}\right)\right]} = \frac{1}{\mathrm{Re}[Z_i]} = \frac{1}{R_{\mathrm{Si1}}} + \omega^2 C^2_{\mathrm{Si1}} R_{\mathrm{Si1}} \tag{7a}$$

$$\frac{-1}{\mathrm{Im}\left[1/\left(Y^{\ell}_{11}+Y^{\ell}_{12}\right)\right]} = \frac{-1}{\mathrm{Im}[Z_i]} = \left(\frac{1}{\omega C_{\mathrm{ox1}}} + \frac{\omega C_{\mathrm{Si1}}}{1/R^2_{\mathrm{Si1}} + \omega^2 C^2_{\mathrm{Si1}}}\right)^{-1}. \tag{7b}$$

Moreover, a further investigation, as shown in Fig. 6, indicates that $(-1/\mathrm{Im}[Z_i])$ shows a good linear variation, whereas $(1/\mathrm{Re}[Z_i])$ is almost invariant as frequency is changed in $f_1 \le f \le f_2$. These relationships exist since both $1/\omega C_{\mathrm{ox1}}$ and $1/\omega C_{\mathrm{Si1}}$ are relatively high impedances in comparison with R_{Si1} in the band. Equation (7b) is therefore simplified as

$$\frac{-1}{\mathrm{Im}\left[1/\left(Y^{\ell}_{11}+Y^{\ell}_{12}\right)\right]} = \frac{-1}{\mathrm{Im}[Z_i]} \approx \omega C_{\mathrm{ox1}}. \tag{8}$$

From the linear regression in (8) in $f_1 \le f \le f_2$, C_{ox1} can then be extracted. A similar treatment can be applied to the right part of the lower subcircuit to extract C_{ox2} by using the Y^{ℓ}_{22} data. In addition, it is worthy mentioning that R_{Si1} could be comparable with $1/\omega C_{\mathrm{Si1}}$ when a high-resistivity silicon substrate is considered. In such a scenario, the linear variation of $(1/\mathrm{Re}[Z_i])$ with regard to ω^2, as characterized by (7a), can be plotted to extract R_{Si1} and C_{Si1}. With the obtained R_{Si1} and C_{Si1}, C_{ox1} is then calculated from (7b).

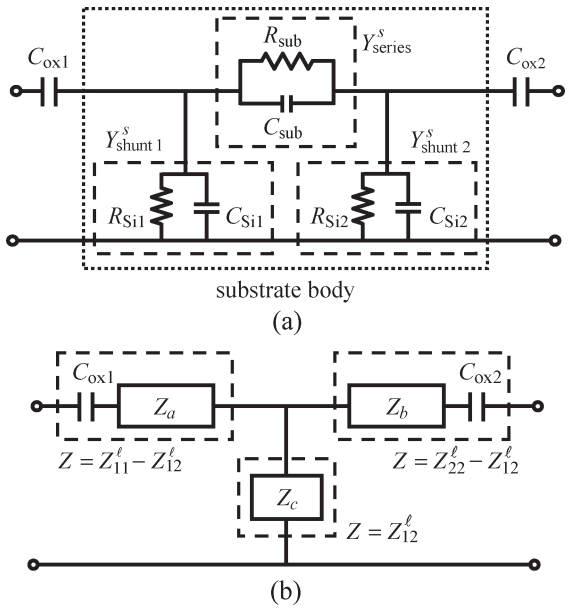

Fig. 7. Representation of the lower subcircuit by (a) a combination of the substrate body and $C_{\mathrm{ox1,2}}$, and (b) an equivalent T-network.

D. Extraction of R_{Si}, C_{Si}, R_{sub}, and C_{sub}

Having determined C_{ox1} and C_{ox2}, the remaining elements $R_{\mathrm{Si1,2}}$, $C_{\mathrm{Si1,2}}$, R_{sub}, and C_{sub} are next extracted over $f \ge f_2$. As shown in Fig. 7(a), the lower subcircuit can be treated as a combination of the substrate body and $C_{\mathrm{ox1,2}}$, where the substrate body is formed by a π-network with the series admittance $Y^s_{\mathrm{series}} = 1/R_{\mathrm{sub}} + j\omega C_{\mathrm{sub}}$ and the two shunt ones $Y^s_{\mathrm{shunt1,2}} = 1/R_{\mathrm{Si1,2}} + j\omega C_{\mathrm{Si1,2}}$. By using an equivalent T-network with the series impedances $Z_{a,b}$ and the shunt one Z_c to model the substrate body, the whole lower subcircuit can be represented by a T-network, as shown in Fig. 7(b). One then obtains $Z_a = Z^{\ell}_{11} - Z^{\ell}_{12} - (j\omega C_{\mathrm{ox1}})^{-1}$, $Z_b = Z^{\ell}_{22} - Z^{\ell}_{12} - (j\omega C_{\mathrm{ox2}})^{-1}$, and $Z_c = Z^{\ell}_{12}$, where Z^{ℓ}_{11}, Z^{ℓ}_{22}, and Z^{ℓ}_{12} are the Z-parameters of the lower subcircuit; they can be readily computed by the Y-matrix of the lower subcircuit $[Y^{\ell}]$ obtained in Section II-C. Finally, by applying the T to π transformation, the T-network of the substrate body can be transformed into the desired π equivalent circuit to find the admittances $Y^s_{\mathrm{shunt1,2}}$ and Y^s_{series}, which leads to

$$Y^s_{\mathrm{series}} = 1/R_{\mathrm{sub}} + j\omega C_{\mathrm{sub}} = Z_c/F \tag{9a}$$

$$Y^s_{\mathrm{shunt1}} = 1/R_{\mathrm{Si1}} + j\omega C_{\mathrm{Si1}} = Z_b/F \tag{9b}$$

$$Y^s_{\mathrm{shunt2}} = 1/R_{\mathrm{Si2}} + j\omega C_{\mathrm{Si2}} = Z_a/F \tag{9c}$$

where $F = Z_a Z_b + Z_b Z_c + Z_c Z_a$. The elements $R_{\mathrm{Si1,2}}$, $C_{\mathrm{Si1,2}}$, R_{sub}, and C_{sub} can be further extracted. Fig. 8 shows the calculated Y^s_{series} and $Y^s_{\mathrm{shunt1,2}}$ as functions of frequency. Frequency-independent results for $\mathrm{Re}[Y^s_{\mathrm{series}}]$ and $\mathrm{Re}[Y^s_{\mathrm{shunt1,2}}]$, which correspond to $1/R_{\mathrm{sub}}$ and $1/R_{\mathrm{Si1,2}}$, are clearly observed in $f \ge f_2$. Meanwhile, it is found that the variations of $\mathrm{Im}[Y^s_{\mathrm{series}}]$ and $\mathrm{Im}[Y^s_{\mathrm{shunt1,2}}]$ with regard to frequency exhibit good linear behavior at high frequencies. The elements C_{sub} and $C_{\mathrm{Si1,2}}$ can be then simply extracted from the slopes of these linear curves.

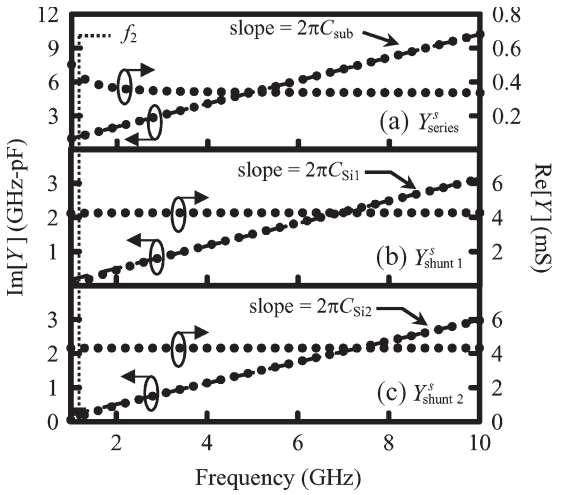

Fig. 8. $Y^s_{\rm series}$ and $Y^s_{\rm shunt1,2}$ as functions of frequency.

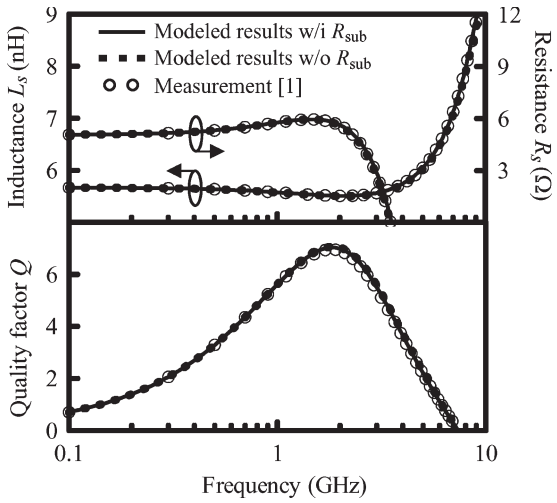

Fig. 9. Comparison of measured and modeled inductance, resistance, and quality factor for the tested 4.5-turn CMOS square spiral inductor. Line width $W = 14.5$ μm, line spacing $S = 2$ μm, and inner radius $R = 60$ μm.

TABLE I
MODEL PARAMETERS FOR THE TESTED 4.5-TURN SQUARE SPIRAL INDUCTOR. LINEWIDTH $W = 14.5$ μm, LINE SPACING $S = 2$ μm, AND INNER RADIUS $R = 60$ μm

Model Parameters	This work	Optimized Values [1]	Reference [19]
L_{s0} (nH)	5.42	5.42	5.6
L_{s1} (nH)	2.94	2.92	3.3
R_{s0} (Ω)	7.14	7.15	7.0
R_{s1} (Ω)	17.37	17.27	18.5
$C_{\rm ox1}$ (fF)	158.4	161.5	167
$C_{\rm ox2}$ (fF)	150.1	152.1	164
$R_{\rm Si1}$ (Ω)	234.2	238.2	111
$R_{\rm Si2}$ (Ω)	231.5	232.1	111
$C_{\rm Si1}$ (fF)	52.51	49.7	27.3
$C_{\rm Si2}$ (fF)	49.24	47.8	27.3
$R_{\rm sub}$ (Ω)	2.9 k	5.7 k	236.9
$C_{\rm sub}$ (fF)	162.9	155.8	56.9

TABLE II
MODEL PARAMETERS FOR THE 2.5- AND 6.5-TURN INDUCTORS. LINEWIDTH $W = 14.5$ μm, LINE SPACING $S = 2$ μm, AND INNER RADIUS $R = 60$ μm

Model Parameters	Extracted results / Optimized values [1]	
	2.5-turn	6.5-turn
L_{s0} (nH)	1.87 / 1.87	11.51 / 11.49
L_{s1} (nH)	1.85 / 1.84	5.03 / 4.92
R_{s0} (Ω)	4.11 / 4.12	10.56 / 10.71
R_{s1} (Ω)	14.33 / 14.20	27.10 / 26.13
$C_{\rm ox1}$ (fF)	89.3 / 91.8	234.4 / 236.8
$C_{\rm ox2}$ (fF)	87.2 / 89.5	227.1 / 228.4
$R_{\rm Si1}$ (Ω)	366.3 / 372.1	146.1 / 147.6
$R_{\rm Si2}$ (Ω)	365.1 / 369.4	143.1 / 142.8
$C_{\rm Si1}$ (fF)	23.3 / 24.1	62.5 / 63.2
$C_{\rm Si2}$ (fF)	23.2 / 24.0	60.9 / 61.9
$R_{\rm sub}$ (Ω)	1.1 k / 1.6 k	6.1 k / 18.6 k
$C_{\rm sub}$ (fF)	100.9 / 94.8	297.6 / 291.7

III. RESULTS AND DISCUSSION

A. Comparison of the Extracted Results and Published Data

Table I lists the extracted model parameters for the inductor tested in Section II. The results are compared with the optimization solutions in [1] and the data by an alternative extraction technique in [19]. It can be seen that our results are very close to the optimization solutions. The only significant deviation is the value of $R_{\rm sub}$. Note that the parallel $R_{\rm sub} - C_{\rm sub}$ network is used to model the lateral coupling among the spiral metal lines. The coupling is dominated by $R_{\rm sub}$ at low frequencies and by $C_{\rm sub}$ at high frequencies [1], [22]. The accuracy of $R_{\rm sub}$ value is therefore important only at relatively low frequencies, where, at the same time, the characteristics of the whole inductor circuit are mainly governed by the upper subcircuit (L_{s0}, R_{s0}, L_{s1}, and R_{s1}) since $C_{\rm ox1}$ and $C_{\rm ox2}$ block low-frequency signals. Thus, it is reasonable to conclude that the accuracy of $R_{\rm sub}$ value would not be critical to the prediction of the inductor characteristics.

Based on the extracted lumped circuit element values, Fig. 9 shows the simulated responses of the key characteristics of the inductor, including the series inductance $L_s = {\rm Im}[-1/Y^m_{12}]/\omega$, series resistance $R_s = {\rm Re}[-1/Y^m_{12}]$, and quality factor $Q = -{\rm Im}[Y^m_{11}]/{\rm Re}[Y^m_{11}]$ and compared with the measured data [1]. The results with removing the $R_{\rm sub}$ is also plotted for comparison. Very good agreement between the simulations and measurements can be observed in the whole frequency range of interest. The root-mean-square deviations for L_s, R_s, and Q are 0.30%, 1.73%, and 1.38%, respectively. Although not shown in this paper, good coincidence between the simulation and measurement for the S-parameters has also been examined. In addition, it is found that the results predicted by the model without $R_{\rm sub}$ are almost identical to those calculated by the original enhanced model. This observation justifies the trivial effect of $R_{\rm sub}$ on the inductor performance. The enhanced circuit model can be therefore further simplified by eliminating $R_{\rm sub}$ with little cost.

The proposed method has further been checked by investigating inductors with different numbers of turns. Table II compares the extracted model parameters for inductors with

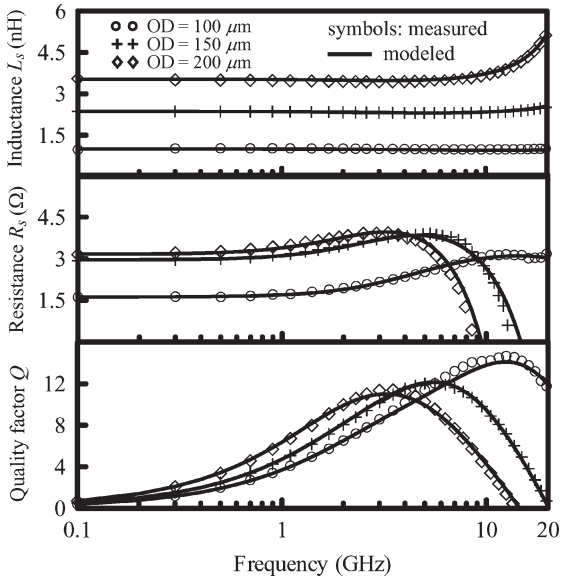

Fig. 10. Comparison of measured and modeled inductance, resistance, and quality factor for 0.13-μm CMOS circular spiral inductor with various outer diameters. Coil number $N = 3.5$, linewidth $W = 6$ μm, and line spacing $S = 2$ μm.

2.5 and 6.5 turns given in [1]. Again, the results by the proposed approach have close agreement with the optimization for both the examples.

B. Experimental Verification

To allow for actual industrial applications, three 3.5-turn circular spirals with the outer diameters (ODs) being 100, 150, and 200 μm have been fabricated and measured to perform the experimental verification of the proposed technique. These inductors were implemented in the UMC 0.13-μm 1P8M mixed-mode/RF CMOS process. The spirals with metal thickness being 2 μm were fabricated on the metal-eight layer, and the underpass was deposited on the metal-seven layer. The linewidth W and line spacing S are 6 and 2 μm, respectively. Moreover, the measured raw data are de-embedded with a two-step (open and short) procedure [23] to remove the undesired pad parasitics. Fig. 10 shows the comparison of the modeled and measured L_s, R_s, and Q of the tested samples. It is seen that the modeled results based on the extracted parameters fit accurately to the measurement data over a wide frequency range from 0.1 to 20 GHz, indicating the wideband modeling capability of the proposed extraction technique, as well as the enhanced model.

C. Applicability to Other IC Fabrication Technology

In addition to the aforementioned CMOS inductors, the modeling of inductors implemented by other IC fabrication technology is also considered. Fig. 11 shows the L_s, R_s, and Q of an eight-turn octagonal spiral fabricated by the BiCMOS7 process [8]. The linewidth W, line spacing S, and outer diameter OD of the considered inductor are 4, 3, and 160 μm, respectively. It is observed that the results simulated by the enhanced model with the proposed parameter-extraction method match well with the measurements in [8]. This indicates

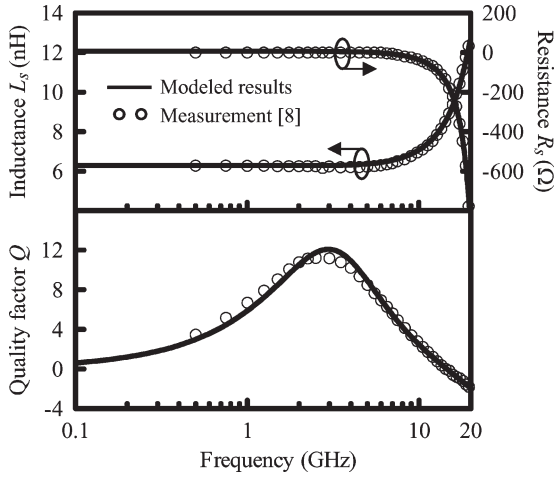

Fig. 11. Comparison of measured and modeled inductance, resistance, and quality factor for an eight-turn BiCMOS7 octagonal spiral inductor. Linewidth $W = 4$ μm, line spacing $S = 3$ μm, and outer diameter OD $= 160$ μm.

that the presented approach and the enhanced circuit model are suitable for dealing with various RFIC inductors.

IV. Conclusion

A systematic technique for accurately extracting model parameters of on-chip spiral inductors has been presented. By introducing suitable approximations, the circuit elements in the model can be analytically extracted in different frequency bands using the network analysis. The validation and capability of the proposed extraction method have been demonstrated by the models of square and circular CMOS spiral and octagonal BiCMOS7 spiral inductors. Moreover, it is found that the lateral resistive coupling $R_{\rm sub}$ has negligible effects on the prediction of inductor characteristics. The enhanced circuit model can be therefore further simplified by eliminating $R_{\rm sub}$ without sacrificing the model accuracy.

Acknowledgment

The authors would like to thank the staff members of UMC for the fabrication and measurement of the test samples and the reviewers for the valuable comments that helped to improve the content of this paper.

References

[1] J. Gil and H. Shin, "A simple wide-band on-chip inductor model for silicon-based RF ICs," *IEEE Trans. Microw. Theory Tech.*, vol. 51, no. 9, pp. 2023–2028, Sep. 2003.

[2] J. R. Long and M. A. Copeland, "The modeling, characterization, and design of monolithic inductors for silicon RF ICs," *IEEE J. Solid State Circuits*, vol. 32, no. 3, pp. 357–369, Mar. 1997.

[3] A. M. Niknejad and R. G. Meyer, "Analysis, design, and optimization of spiral inductors and transformers for Si RF ICs," *IEEE J. Solid State Circuits*, vol. 33, no. 10, pp. 1470–1481, Oct. 1998.

[4] C. P. Yue and S. S. Wong, "Physical modeling of spiral inductors on silicon," *IEEE Trans. Electron Devices*, vol. 47, no. 3, pp. 560–568, Mar. 2000.

[5] I. C. H. Lai and M. Fujishima, "A new on-chip substrate-coupled inductor model implemented with scalable expressions," *IEEE J. Solid State Circuits*, vol. 41, no. 11, pp. 2491–2499, Nov. 2006.

[6] D. Melendy, P. Francis, C. Pichler, K. Hwang, G. Srinivasan, and A. Weisshaar, "A new wide-band compact model for spiral inductors

in RFICs," *IEEE Electron Device Lett.*, vol. 23, no. 5, pp. 273–275, May 2002.
[7] F. Rotella *et al.*, "A broad-band lumped element analytic model incorporating skin effect and substrate loss for inductor and inductor like components for silicon technology performance assessment and RFIC design," *IEEE Trans. Electron Devices*, vol. 52, no. 7, pp. 1429–1441, Jul. 2005.
[8] S. K. Mandal, A. De, A. Patra, and S. Sural, "A wide-band lumped element compact CAD model of Si-based planar spiral inductor for RFIC design," in *Proc. 19th Int. Conf. VLSI Design*, 2006, pp. 619–624.
[9] Y. Cao *et al.*, "Frequency-independent equivalent-circuit model for on-chip spiral inductors," *IEEE J. Solid State Circuits*, vol. 38, no. 3, pp. 419–426, Mar. 2003.
[10] A. C. Watson, D. Melendy, P. Francis, K. Hwang, and A. Weisshaar, "A comprehensive compact-modeling methodology for spiral inductors in silicon-based RFICs," *IEEE Trans. Microw. Theory Tech.*, vol. 52, no. 3, pp. 849–857, Mar. 2004.
[11] K.-Y. Lee, S. Mohammadi, P. K. Bhattacharya, and L. P. B. Katehi, "A wideband compact model for integrated inductors," *IEEE Microw. Wireless Compon. Lett.*, vol. 16, no. 9, pp. 490–492, Sep. 2006.
[12] J.-C. Guo and T.-Y. Tan, "A broadband and scalable model for on-chip inductors incorporating substrate and conductor loss effects," *IEEE Trans. Electron Devices*, vol. 53, no. 3, pp. 413–421, Mar. 2006.
[13] T. S. Horng, J. K. Jau, and Y. S. Tsai, "Equivalent circuit for broadband modelling of on-chip spiral inductors up to millimeter-wave frequencies," *Electron. Lett.*, vol. 41, no. 15, pp. 838–840, Jul. 2005.
[14] T. S. Horng, J. K. Jau, Y. S. Tsai, and C. S. Huang, "A decomposition and reconstruction scheme for broadband modeling of on-chip passive components using the modified T-equivalent circuit topology," in *Proc. IEEE Radio Freq. Integr. Circuits Symp. Dig.*, 2005, pp. 299–302.
[15] C. Zhen and G. Lihui, "Application of the genetic algorithm in modeling RF on-chip inductors," *IEEE Trans. Microw. Theory Tech.*, vol. 51, no. 2, pp. 342–346, Feb. 2003.
[16] J. Kolstad, C. Blevins, J. M. Dunn, and A. Weisshaar, "A new circuit augmentation method for modeling of interconnects and passive components," *IEEE Trans. Adv. Packag.*, vol. 29, no. 1, pp. 67–77, Feb. 2006.
[17] F. Huang, N. Jiang, and E. Bian, "Characteristic-function approach to parameter extraction for asymmetric equivalent circuit of on-chip spiral inductors," *IEEE Trans. Microw. Theory Tech.*, vol. 54, no. 1, pp. 115–119, Jan. 2006.
[18] F. Y. Huang, J. X. Lu, D. M. Jiang, X. C. Wang, and N. Jiang, "A novel analytical approach to parameter extraction for on-chip spiral inductors taking into account high-order parasitic effect," *Solid State Electron.*, vol. 50, no. 9/10, pp. 1557–1562, Sep./Oct. 2006.
[19] M. Kang, J. Gil, and H. Shin, "A simple parameter extraction method of spiral on-chip inductors," *IEEE Trans. Electron Devices*, vol. 52, no. 9, pp. 1976–1981, Sep. 2005.
[20] K. Han *et al.*, "Complete high-frequency thermal noise modeling of short-channel MOSFETs and design of 5.2-GHz low noise amplifier," *IEEE J. Solid State Circuits*, vol. 40, no. 3, pp. 726–735, Mar. 2005.
[21] N.-J. Oh and S.-G. Lee, "Current reused *LC* VCOs," *IEEE Microw. Wireless Compon. Lett.*, vol. 15, no. 11, pp. 736–738, Nov. 2005.
[22] W. Jin, Y. Eo, J. I. Shim, W. R. Eisenstadt, M. Y. Park, and H. K. Yu, "Silicon substrate coupling noise modeling, analysis, and experimental verification for mixed signal integrated circuit design," in *Proc. IEEE MTT-S Int. Microw. Symp. Dig.*, 2001, pp. 1727–1730.
[23] Y. Cheng, M. J. Deen, and C.-H. Chen, "MOSFET modeling for RF IC design," *IEEE Trans. Electron Devices*, vol. 52, no. 7, pp. 1286–1303, Jul. 2005.

Hao-Hui Chen (M'99) received the B.S. degree in physics from the National Central University, Taoyuan, Taiwan, R.O.C., in 1991 and the Ph.D. degree in communication engineering from the National Chiao Tung University, Hsinchu, Taiwan, in 1998.

From 1998 to 2008, he was with the Department of Electronic Engineering, Huafan University, Taipei, Taiwan. Since 2008, he has been with the Department of Electronic Engineering, National Kaohsiung First University of Science and Technology, Kaohsiung, Taiwan, where he is currently an Associate Professor. His research interests include passive component and circuit designs for RFICs, RF and microwave circuit designs, RFIC device modeling, planar antenna design, and computational electromagnetics.

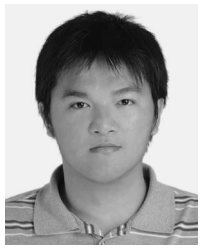

Huai-Wen Zhang received the B.S.E.E. degree and M.S. degree in communication engineering from the National Chiao Tung University, Hsinchu, Taiwan, R.O.C., in 2004 and 2006, respectively.

He is currently with the United Microelectronics Corporation, Hsinchu. His research interests include active and passive RF devices and advance processes for RFICs.

Shyh-Jong Chung (M'92–SM'06) received the B.S.E.E. and Ph.D. degrees from the National Taiwan University, Taipei, Taiwan, R.O.C., in 1984 and 1988, respectively.

Since 1988, he has been with the Department of Communication Engineering, National Chiao Tung University, Hsinchu, Taiwan, where he is currently a Professor. From 1995 to 1996, he was a Visiting Scholar with the Department of Electrical Engineering, Texas A&M University, College Station. His areas of interest include the design and applications of active and passive planar antennas, communications in intelligent transportation systems, LTCC-based RF components and modules, packaging effects of microwave circuits, and c electromagnetics.

Jen-Tsai Kuo (S'88–M'92–SM'04) received the Ph.D. degree from the Institute of Electronics, National Chiao Tung University (NCTU), Hsinchu, Taiwan, R.O.C., in 1992.

Since 1984, he has been with the Department of Communication Engineering, NCTU, where he is currently a Professor. In 1995–1996, he was a Visiting Scholar with the Electronic Engineering Department, University of California, Los Angeles. His research interests include analysis and design of microwave integrated circuits and numerical techniques in electromagnetics.

Dr. Kuo is currently an Editorial Board member of the IEEE TRANSACTIONS ON MICROWAVE THEORY AND TECHNIQUES and the IEEE MICROWAVE AND WIRELESS COMPONENTS LETTERS. He was one of the recipients of the best paper award of the 2002 National Telecommunication Conference, Taiwan, and the Asia Pacific Microwave Conference Prize, Bangkok, Thailand, December 2007. He also received the Taiwan Citation Laureate 2006 from the Thomson Scientific and the 2007 Distinguished Research Award from the National Science Council, Taiwan.

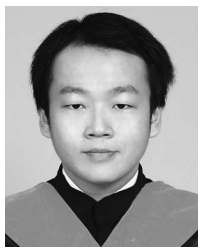

Tzung-Chi Wu was born in Yunlin, Taiwan, R.O.C., in 1982. He received the B.S.E.E. degree from the Technology and Science Institute of Northern Taiwan, Taipei, Taiwan, in 2005.

He is currently with Inventec Corporation, Taoyuan, Taiwan. His current research interests focus on the modeling of on-chip spiral inductors.